University of Strathclyde Glasgow

Strathprints Institutional Repository

Stack, Margaret and Mathew, Mathew T and Hodge, C. (2011) *Micro-abrasion-corrosion interactions of Ni-Cr/WC based coatings : Approaches to construction of tribo-corrosion maps for the abrasion-corrosion synergism.* Electrochimica Acta, 56 (24). pp. 8249-8259. ISSN 0013-4686

Strathprints is designed to allow users to access the research output of the University of Strathclyde. Copyright © and Moral Rights for the papers on this site are retained by the individual authors and/or other copyright owners. You may not engage in further distribution of the material for any profitmaking activities or any commercial gain. You may freely distribute both the url (http://strathprints.strath.ac.uk/) and the content of this paper for research or study, educational, or not-for-profit purposes without prior permission or charge.

Any correspondence concerning this service should be sent to Strathprints administrator: mailto:strathprints@strath.ac.uk

http://strathprints.strath.ac.uk/

University of Strathclyde Glasgow

Stack, M.M. and Mathew, M.T. and Hodge, C. (2010) Micro-abrasion-corrosion interactions of Ni-Cr/WC based coatings: approaches to construction of tribo-corrosion maps for the abrasion-corrosion synergism. Electrochimica Acta . ISSN 0013-4686

http://strathprints.strath.ac.uk/27188/

This is an author produced version of a paper published in Electrochimica Acta . ISSN 0013-4686. This version has been peer-reviewed but does not include the final publisher proof corrections, published layout or pagination.

Strathprints is designed to allow users to access the research output of the University of Strathclyde. Copyright © and Moral Rights for the papers on this site are retained by the individual authors and/or other copyright owners. You may not engage in further distribution of the material for any profitmaking activities or any commercial gain. You may freely distribute both the url (http://strathprints.strath.ac.uk) and the content of this paper for research or study, educational, or not-for-profit purposes without prior permission or charge. You may freely distribute the url (http://strathprints.strath.ac.uk) of the Strathprints website.

Any correspondence concerning this service should be sent to The Strathprints Administrator: eprints@cis.strath.ac.uk

Micro-abrasion-corrosion interactions of Ni-Cr/WC based coatings: approaches to construction of tribo-corrosion maps for the abrasion-corrosion synergism

M.M. Stack, M. T. Mathew and C. Hodge

Department of Mechanical Engineering,

University of Strathclyde, 75 Montrose St.,

Glasgow, G1 1XJ, UK

Phone-+44-141-5483754, Fax-+44-141-5525105

E-mail margaret.stack@strath.ac.uk

Abstract

The process of micro-abrasion-corrosion has been the subject of much research in recent years due to the fact that the action of micron sized particles, typically less than 10 um in diameter, can cause significant degradation of materials in many diverse environments involving aqueous corrosion. Cermet based coatings are often used to combat micro-

abrasion-corrosion, but has been little work carried out to characterize the performance of such coatings exposed to micro-abrasion-corrosion or to provide a basis for coating optimisation. In addition, a basis for defining the various micro-abrasion-corrosion interactions has not been suggested to date.

In this study the micro-abrasion-corrosion performance of a Ni-Cr/WC coating was assessed and compared to the performance of the steel substrate. The results were used to identify regimes of micro-abrasion as a function of applied load and pH of the solution. In addition, micro-abrasion-corrosion maps were constructed based on the results, showing the variation between micro-abrasion-corrosion regimes, as a function of applied load and pH of the solution.

1.0 Introduction

Micro-abrasion is a common materials limiting issue in industrial applications ranging from bio-medical conditions to space [1-7]. For PVD duplex and single-layered TiAlN and TiN coatings, the process of micro-abrasion has been extensively studied on the performance of such coatings[8,9]. Moreover, further studies have been carried out for pure metals and WC-HVOF coatings to investigate the micro-abrasive behaviour for different conditions[10]. Other studies have addressed the micro-abrasive behaviour of soft materials, soda-lime glasses, prosthetics and materials used for dental implants and prostheses[11-13].

In the literature, there has, been little work carried out to study the effects of micro-abrasion on the corrosion rate of materials, especially on coatings. Such effects are important to characterize because micro-abrasion in bio-medical and industrial applications typically occurs in corrosive solutions in which the pH and electrochemical potential may vary significantly [2-6]. Understanding the combined effects of the tribological and corrosion variables, for micro-abrasion-corrosion, as in sliding wear-corrosion[14], is critically important for optimizing materials selection and tribo-corrosion parameters in such conditions.

For WC cermet based coatings, whilst the high hardness property of the WC is well understood, it is also recognized that the hard carbides fail to show good fatigue life on their own and thus the need for mixing them with binders in metal matrice structures arises. It has been found that increasing the ratio of carbides to binders in such metal matrices results in greater abrasive resistance at the expense of decreased ductility, such that various windows of conditions can be identified, where additions of reinforcement can be beneficial, or deleterious, for optimum abrasive resistance [15].

Thus, introduction of binder phases significantly alters the corrosion properties of the material and, coupled with the abrasive-corrosive interaction, adds a further degree of complexity into the process. Chromium and Nickel in particular are known to improve

significantly the corrosion resistance to the parent compound and therefore alloys of such metals are commonly used for the matrix material. [16-17].

For MMCs, it is proposed that corrosion in many cases may aid in the abrasive wear rate of sintered carbides through so-called synergistic effects. It does so by dissolving the binder phase which in turn allows easier removal of the hard carbides by abrasive wear processes[18-19]. Studies [20] have shown that preferential corrosion at the interface between the WC and Co phases in WC-Co sintered carbides, and of the WC phase, occurs in aqueous conditions and that a stable hydroxide film forms on the Co binder at higher alkaline pH values; however this protective film reduces in stability as the pH decreases [21]. In these studies, abrasive wear was found to be the dominant force in such interactions, together with dissolution of the WC phases [22-23]. However, in some cases, the presence of corrosive action was found to have a negative synergism, leading to lower wear rates [24].

Just as corrosion can aid in abrasive wear rate, the abrasive action has been recorded to aid in corrosive attack, and hence leading to a synergistic relationship between the mechanical and chemical interactions. In particular, corrosive wear rates have been observed to be some order of magnitude greater in conditions of erosion-corrosion, compared with static [25] conditions, with the corrosive wear rates for WC-based hardmetals changing at various potential values.

Advances in the study of micro-abrasion have lead to the construction of engineering maps to characterize the wear mechanisms [6-8]. Such maps provide a means of identifying the wear regime and levels of wastage. However, to date, there have been few attempts to construct such diagrams to identify the synergism between the tribological and corrosion process, although some recent work has focused on development of synergistic mechanism maps for WC based coatings for erosion-corrosion and for Co-Cr alloys exposed to micro-abrasion-corrosion.

In this work, the micro abrasion-corrosion behaviour of a ceramic against a Ni-Cr/ WC b coating was assessed in an aqueous slurry solutions having at various pH values (containing SiC particles) over a range of applied loads. The results were used to establish regimes of micro-abrasion-corrosion. Micro abrasion-corrosion maps, showing mechanisms of degradation, wastage and synergistic effects were constructed as a function of applied load and pH of the solutions, based on the results. The significance of such maps in tailoring coatings for micro-abrasion-corrosion resistance is addressed in this paper.

2.0 Experimental details

Micro-abrasion tests were performed with a commercially available apparatus, the TE-66, micro-abrasion tester Figure. 1 (Plint and partners (Phoenix, UK). The details of the

experimental rig are as follows. A 25mm ceramic ball is located between two-coaxial shafts each carried in support bearing.

A shaft was driven by a variable speed DC geared motor and a batch counter is provided to measure and control the number of shaft revolutions. A peristaltic pump head was connected to the other end of the shaft and this was used for providing slurry feed to the contact. The test sample was clamped onto a platform, which is fitted to the pivoted L-shaped arm. The arm was rotated around a pivot until the sample comes into contact with the ball and the load is applied by adding dead weights to a cantilever arm.

The arm, which holds the sample, could be moved horizontally in order that several tests on a single sample specimen can be carried out. This configuration had the advantage of accurate control of both normal load (to an accuracy of $\pm$0.01N) and sliding speed. The sample was then removed from the apparatus and the diameter of the resulting wear scars were measured with a profile projector and optical microscope.

The material of the ball used was ceramic (SiN). The sample Ni-Cr/WC-lasercarb coating surfaces were ground and polished by conventional metallographic methods before testing.

The coating (thickness of 1166 μm) was deposited by a Lasercarb process. (Lasercarb is a process developed by the R&D department of Technogenia. The principle involves using the energy of a CO_2 laser beam to fuse the added metal ("Lasercarb" carbide

powders), and the base metal very slightly –a Thermally Affected Zone (TAZ) of a few microns.

Following the test, the worn samples were examined by optical, scanning electron microscopy in addition to profilometric methods. Repeat tests were carried out at various loads; the error in the experimental data is estimated to be $\pm$ 12%.

The wear volume was calculated using the standard technique [9] for measuring the wear scar of spherical geometry [3] i.e. the geometry of the wear scar is assumed to reproduce the spherical geometry of the ball, and the wear volume (V) may then be calculated by measurement of either the crater diameter (b) or its depth (h).

$$V \approx \pi b^4 / 64\, R \quad \text{For } b \ll R \quad \ldots\ldots\ldots\ldots\ldots(1)$$

$$V \approx \pi\, h^2 R \quad \text{For } h \ll R \quad \ldots\ldots\ldots\ldots\ldots(2)$$

For estimation of the corrosion rate, the sample was connected to the working electrode and a reference electrode by capillary tube in order to make contact with the circuit. A Pt-Ti wire mesh was used as an auxiliary electrode. To ensure that all other parts were insulated, the sample was painted with electrically nonconductive paint except at the point of interaction. The clamps and plate, which hold the sample, were made of non-conducting polymer. Potential control for corrosion studies was carried out using a Gill AC electrochemical interface (ACM instruments, UK).

Following an initial stabilization period at –1.0 V (SCE) for 120 s, polarization curves during simultaneous micro-abrasion, were measured from –1.5 to +0.5 V at a sweep rate at 2 mV s^{-1}. In this apparatus, the solution was exposed to air. Thus, although the polarization curves show the received data, for calculation of Kc, the measured current densities were corrected, at specific potentials, for the presence of reducing cathodic currents (i.e. by subtraction of the oxygen reduction current at –1.0 V, SCE).

Micro-abrasion corrosion tests were carried out at various applied loads 1,2,3,4,5 N at a constant sliding distance of 3000 rev (235.50 m) and fixed potential -0.20 V. The corrosion rates (Kc) during micro-abrasion corrosion were obtained from the current densities at potential of -0.2 V (SCE), with corrosive slurry having various pH values i.e. 2, 5.5, 9.7, 13.5. The total mass losses due to microabrasion wear and corrosion (Kac) at the above pHs were measured after 30 minutes.

3.0 Results

3.1 Electrochemical Polarization behavior

Polarization curves are shown in Fig. 2 at various pH values for two experimental methods, (a) Corrosion only (Beaker experiment) (b) Micro-abrasion-corrosion experiment at 5N. It is interesting to note that from Fig. 2 (a), at pH 6, the surface passivated earlier than for the other pH values, with the current densities being highest for pH 13.5. It is clear from the polarization curves for pHs 2, 6 and 9.7, that a passivation transition occurred in such conditions, mid-way through the initial

passivation process. At pH 13.5, an active dissolution process was observed except at the highest potentials.

The polarization curves for micro-abrasion corrosion, Fig. 2(b), showed significant differences to the beaker test curve. There was less evidence of passivation for pH 6 and 13.5, and in both cases the micro-abrasion-corrosion process appeared to be dominated by active dissolution. At pH 2 and 9.7, some slight evidence of passivation and transpassive behaviour was observed, but to a much lesser extent than that which is observed for Fig. 2(a)

The polarization curves at pH 9.7, at various loads, Fig. 2©, indicated that the passive currents increased incrementally with applied load. It is interesting to note that the zero current potential (Ecorr) tended to change with increases in applied load, with a marginal reduction at the lower loads. A slight "kink" in the passive current curve was also observed at the various loads.

3.2 Mass Change data

The mass change data may be explained by defining the following terms, using the wear-corrosion analysis developed by Yue and Shi [10]:

If: $K_{ac} = K_a + K_c$ …… (1)

where, Kac is the total micro-abrasion-corrosion, Ka is the total micro-abrasion rate, and Kc is the total corrosion rate.

Ka can be written as Kao + Δ Ka, i.e.:

$$Ka = Kao + \Delta Ka \quad \ldots\ldots\ldots\ldots\ldots\ldots\ldots\ldots (2)$$

where Kao is the micro-abrasion rate in the absence of corrosion, Δ Ka is the effect of corrosion on the micro-abrasion.

Kc can be written as Kco + ΔKc, i.e:

$$Kc = Kco + \Delta Kc \quad \ldots\ldots\ldots\ldots\ldots\ldots\ldots\ldots (3)$$

where Kco is the corrosion rate in the absence of wear, ΔKc is the effect of micro-abrasion on the corrosion, or the enhancement of corrosion due to the micro-abrasion process.

Hence, the total micro-abrasion – corrosion rate can be given as follows:

$$Kac = Kao + \Delta Ka + Kco + \Delta Kc \quad \ldots\ldots\ldots (4)$$

The results of the various contributions to weight change are given in Table 3 and Figure 3. The corrosion rate data, Kc, were derived using Faraday's law, e.g.

$Kc=Q/ZF$…….(5)

$Kc=MIt/ZF$…… (6)

where Q is the charge passed, F is Faraday's constant (96500 C mol^{-1}), Z is the number of electrons involved in corrosion process, I, the total current, t the exposure time and M is the molecular weight of the material.

Eq.Wt $= \Sigma (fi * ni) / ai$

fi – Fraction of the elements, ai- atomic weight of individual elements, ni- number of valence electron.

Eq.Wt = 15.75

Eq.Density = Σ (fi * Di)……..Di- Density of individual elements.

Eq.Density- 8.05 (g/cm3)

(It should be noted that equation 5 and 6 rely on a prediction of the oxidation valency for the Ni and Cr, which is approached with difficulty due to the transition from active to passive states for the range of conditions studied above**.** In particular, Chromium has 5 different valence states [25].)

The mass loss due to wear in the absence of corrosion, Kao, was estimated by measuring the mass change in cathodic conditions i.e. at –1.0 V. The corrosion rate data, Kc, were corrected for the oxygen reduction reaction.

Variation of mass loss data, Kac, total micro-abrasion corrosion, Ka, wear due to abrasion, and Kc, wear due to corrosion with variation of load, Figs 3 (a-d), indicated a characteristic peak at intermediate loads for Ka and Kac. For Kc, however, there was little variation of the magnitude of this value with increasing load. The mass loss variation with load for other pH values, Figs. 3 (b-d) respectively indicated that at pH 9.7, the mass loss recorded was highest out of all the pHs studied.

3.3.Micrographs of the coatings and SEM images of the worn surface.

The micrographs of the coating and substrate material, Fig. 4, showed that after cross sectional analysis, the presence of a crack on the coating (possibly introduced during manufacturing). A higher magnification of the structure, Fig. 4(b), indicated the fine grained structure of the coating and the clear difference between the reinforcement and the matrix, Fig. 4(c) was evident. The variation of shape of reinforcement was evident at higher magnifications, Fig. 4(d). .

SEM images of the SiC 4μm abradent used in the test indicated the significant angularity of the abrasive particles, Fig. 5(a). SEM images of the wear scar at various conditions, Fig 5 (b-c), indicated deformation at the surface during the micro-abrasion-corrosion processes.

At 5N, Figs. (d-e), and at pH 5.5, it was interesting to note that there was a lack of significant deformation compared with SEM images at pH 2. The sample surface exposed to corrosion, Fig. 5(f), showed evidence of degradation.

At 5N and pH 9.7, it was shown, Figs.5 (g-i), that high levels of deformation occurred on the surface, due to the chemical and mechanical effects during the micro-abrasion–corrosion process. The surface following corrosion only, indicated the presence of crevice corrosion and dissolution of WC-particles at such pH values.

The wear scar for 5N and pH 13.5, and the surface following corrosion only, at pH 13.5, Figs. 5 (k-l) respectively exhibit significantly less deformation, compared with the results for pH 9.7.

4.0 Discussion

4.1. Polarization curves

It is interesting to note that the polarization curves at various pHs for the corrosion only experiment, exhibit preferential passivation at pH 5.5. The polarization curves also provide evidence of the passivation and repassivation, at all pHs except for pH values of 13.5.

A corrosion map has been constructed based on the results, similar to a classical Pourbaix diagram, and shows the active, passive, immune regime as a function of applied potential, and pH of the solution, Fig. 6. The schematic corrosion map can be related to the Pourbaix diagram of Cr and Ni, where the various stability regimes for the dissolution and passivity are demonstrated, Figs. 7-8. The high mass % of Chromium in the coating

may suggest that the corrosion of Chromium is the rate controlling process in the corrosion mechanism.

Selection of a fixed potential of -0.20 V for the mass change data experiment, is based on the schematic corrosion map Figure 6, where at such potentials, it shows there are transitions from active to passive regimes based on the electrochemical data above, Fig. 2.

4.2. Mass loss data

The results, Fig. 3, show that the micro-abrasion-corrosion increases incrementally with load, consistent with the Archard theory on the effect of applied load on wear rate [11]. However, at intermediate loads there is a pronounced peak in the wear rate. This is attributed to the formation of the ridges and high frictional heating at the interface which results in a noticeable drop in wear rate thereafter.

The corrosion rate generally shows a constant trend as a function of load and pH of the solution. The evidence of a slight reduction in corrosion rate as load increases may be due to the rapid re-passivation kinetics and to a greater thickness of passive films consistent with the polarization data above, Fig. 2.

It should be noted that there is clear evidence of high mass loss data at pH 9.7, which is consistent with SEM images of the wear scar (Figs. 5(g-i). In order to analyze the mechanism of degradation, a schematic diagram of the micro-abrasion corrosion process is shown in Figs 9-10.

The corrosive action encourages the formation of passive films on the surface, which in turn takes part in the abrasion process. The formation of these films and their rapid removal depends on the pH of the solution, applied load and speed of the ball.

There is also slight evidence of crevice corrosion, which is clear from the SEM images of the sample surface for the corrosion only experiment Fig. 5(k) It is interesting to note that the boundary of the carbide grains may be corroded, which leads to rapid dislodging of the WC-grains from the surface, Fig.9. This is observed further in the SEM images at pH 9.7, which leads to a high material loss rate above.

4.3. Micro-abrasion –corrosion mechanism and wastage maps in aqueous conditions

Mechanism Map

Various research groups to date have constructed micro-abrasion maps [1, 6-8, 12] with a number of mechanisms proposed to characterize the wear rate. An attempt has been

made to distinguish between the different corrosion regimes affecting the micro-abrasion as follows,

$$Kc/Ka \leq 0.1 \quad \text{(micro-abrasion)} \quad (5)$$

$$0.1 < Kc/Ka \leq 1 \quad \text{(micro-abrasion- corrosion)} \quad (6)$$

$$1 < Kc/Ka \leq 10 \quad \text{(corrosion-micro-abrasion)} \quad (7)$$

$$Kc/Ka > 10 \quad \text{(corrosion)} \quad (8)$$

The regime criteria is an adaption of criteria used in previous work [13-14]. The resulting map can be seen in Fig. 11, based on Table 3.

The boundaries on the map are established through extrapolating the various regimes based on the individual corrosion and micro-abrasion contributions. The corrosion process may be active or passive depending on the conditions. The map, Fig. 11, indicates that the active-to-passive corrosion transition changes with applied load, consistent with the polarization data, Figure 2. Not surprisingly, dissolution affects the micro-abrasion process at lower pHs. Dissolution-micro abrasion is observed at higher pHs and low pHs as the load increases. Passivation is favoured at intermediate pH values, i.e. from pH 4-6, consistent with the passivation region identified for Cr on the Pourbaix diagram Fig. 7. At the highest pH values, the wear rate is dominated by the abrasive component for all loads tested.

Wastage map

A wastage map has been developed, Fig. 12, for this coating based on the following boundary conditions

Low -	$X \leq 0.002$ mm^3	(9)
Medium	0.002 mm$^3 \leq X < 0.004$ mm^3	(10)
High-	$X \geq 0.004$ mm^3	(11)

where X is wear mass loss in mm^3 (0.002 mm^3 = 1.61 x 10^{-5} g and 0.004 mm^3 = 3.22 x 10^{-5} g). It should be noted that the high wastage zone, identified in Fig. 12, corresponds to the micro-abrasion-dissolution dominated zone in the mechanism map, Fig.11, which indicates that the interaction of micro-abrasion with dissolution is the most deleterious regime for the material.

Synergism map

A tribo-corrosion synergism map [24-25] has been developed based on the following inequalities i.e.

$\Delta Ka/\Delta Kc \leq 0.1$	Additive	(12)
$1 \geq \Delta Ka/\Delta Kc \geq 0.1$	Additive-synergistic	(13)
$\Delta Ka/\Delta Kc \geq 1$	Synergistic	(14)

If the inequalities are negative, then “additive” is changed to “subtractive” and “synergistic” is changed to “antagonistic”.

The map, Fig. 13, based on data in Table 4, indicates that because the corrosion current densities reduced at the various pH values following micro-abrasion, Figs. 2(a-b), a region of subtractive behavior is observed. The presence of third body debris, or particulate matter from the abradent, may have reduced the corrosion current density at the higher pH values. As indicated above, Fig. 9-10, the tribo-corrosion process of such composites is an amalgam of the wide variety of tribo-corrosion interactions involving the Ni-Cr matrix i.e.

(i) WC reinforcement

(ii) Interface between the two phases

(iii) SiC particles

(iv) Presence of third debris arising from the wear process

(v) Deposition of particulate matter involved in the abrasive process

(vi) Differential effects of pH on the stability and dissolution effects of such phases.

Not surprisingly, there is a wide range of tribo-corrosion interactions possible, as indicated above, Figs. 11-13. The antagonistic region between pH 5 and 7, is likely to be due to the passivation of Cr in such conditions, and the transition to the

dissolution affected regime below pH is consistent with the behavior identified on the Pourbaix diagram,. Fig. 7.

At pH 9.7 further analysis of the synergistic effects on the wear process, Fig. 14. The range of values shows that these effects may be very different at various loads. Additional analysis at various pHs and cathodic conditions at -1.0 V, Fig. 15, indicate that the highest value of ΔKa is found at pH 9.7. This indicates that the severity of micro-abrasion-corrosion process, and the synergism between wear and corrosion for such coatings, is critically dependent on the value of pH.

Clearly such maps are an important tool in identifying micro-abrasion-corrosion interactions. Further work will be to investigate how such mapping techniques may be applied to practical applications, where corrosion may have a significant effect on the micro-abrasion process.

5.0 Conclusions

- Effects of applied load and pH of the solution have been studied on the micro-abrasion-corrosion of Ni-Cr/WC-lasercarb coated steel.
- Micro-abrasion-corrosion mechanism, wastage and synergism maps have been constructed based on the results showing transitions between micro-abrasion-corrosion regimes as a function of load and the solution pH.

- An intermediate pH value of 9.7 is consistent with the highest wastage rate for the range of loads and potentials in these environments.

6.0 Acknowledgements

The authors would like to express their gratitude to the late Dr.Len Philips, Weir Pumps (Ltd) Glasgow, UK, for supplying the samples for the study and to Dr. Hosen Jawan, Academic visitor from College of Engineering, University of Al Mrkeb, Libya.

7.0 References

1. Buchananan F.J. and Shipway P.H.; Biomaterials, (2002) 23, pp93-100.
2. Firkins P.J, Tipper J L, Saadatzadeh M.R., Ingham E, Stone M.H., Farrar R., and Fisher J.; Bio-Medical Materials Engineering (2001) 11, 2, pp143-157.

3. Ingram J , Matthews J.B., Pipper J., Stone M., Fisher J. and Ingham J.; Bio-Medical Materials Engineering, (2002) 12, 2, pp177-188.
4. Eisenburgar M and Addy M.; J. Oral Rehabilitation, (2003) 30, 11, pp1076-1080.
5. Attin T., Meyer E, Hellwig E, Burchalla W and Lennon A.M.; Arch. Oral Biology (2003) 48, pp753-759.
6. Trezona R.I., Alsopp, D.N. and Hutchings, I.M.; Wear (1999) 225-229, pp205-214.
7. Stack M.M. and Mathew M.T, Wear (submitted)
8. Stack, M.M.; Mathew, M.; Wear (2003) 255 pp14-22
9. Rutherford,K.L.; and Hutchings,I.M.; Journal Testing and Evaluation, JTEVA, (1997) 25, 2, pp. 250-260
10. Yue, Z, Zhou P and J. Shi in Luedema K.C. Ed., Proc. Conf. Wear of Materials, ASME, New York, 1987, pp763-768.
11. Archard. J.F.; J.Appl.Phys, (1953) 24 p98.
12. Adachi,K. and Hutchings, I.M.; Wear (2003) 255 pp23-29.
13. Stack, M.M.; Zhou, S. and Newman, R.C.; Mater. Sci. Tech (1996) 12, pp261-268.
14. Stack, M.M.; Chi K.; Wear (2003) 255, pp456-465.
15. Development and characterization of composite Ni-Cr+WC cladding L.St Georges 2007
16. http://en.wikipedia.org/wiki/Nickel
17. http://en.wikipedia.org/wiki/Chromium
18. J. Larsen-Basse, Wear (1985) 105, pp257-256

19. P. Shipway, J.J. Hogg, Wear (2005), 259, pp44-51

20. Hochstrasser S, Latkoczy C, Virtanen S, Uggowtizer PJ, Schmutz P. In: Proceedings of the 208th meeting of The Electrochemical Society, Los Angeles, CA, USA, 2005.p.662

21. Hochstrasser S, Muller Y, Latkoczy C, Virtanen S, Schmutz P., Corros Sci (2007) 49, pp2002-20.

21. Thakare MR, Wharton JA, Wood RJK, Menger C, Tribology International (2007), 41 (7), pp 629-639.

22. Mathew M.T, Ariza E, Rocha L.A, Fernandes A.C., Vaz F, Electrochimica Acta (in press)

23. Thakare MR, Wharton JA, Wood RJK, Menger C, Wear (2007), 263 (1-6), pp125-136.

24. Kalish HS, Corrosion of cemented carbides Corrosion, vol.13 9TH edition., ASM International, Ohio, USA, 1987, pp 846-858.

25. Stack M.M. Abd El Badia T.M. (2008), Wear, 264 (9-10), 826-837.

26. Stack, M.M. and Rodling, J. and Mathew, M.T. and Jawan, H. and Park, G. and Hodge, C. (2010) Wear, 269 (5-6). pp. 376-382

Figure captions

1. Schematic diagram of micro-abrasion-corrosion experimental apparatus.

2. Polarisation curves with different pHs (a) Corrosion only (b) Micro-abrasion-corrosion at 5N (c) at pH 9.7 and various loads

3. Variation of wear rate with applied load for the following sliding distances.
   (a) pH 2.
   (b) pH 5.5
   (c) pH 9.7
   (d) pH 13.5

4. Optical micrographs of WC-Lasercarb coated stainless steel

   (a) Cross-sectional micrograph of coating at low magnification
   (b) Micro-structure of substrate material
   (c) Micrograph of coating alone.
   (d) Coating microstructure at high magnification.

5. Scanning electron micrographs of abraded surfaces.

   (a) SiC carbide particles used in the test
   (b) Wear at ,5N, pH 2.

(c) Corrosion only, pH 2.

(d) Wear at 5N, pH 5.5

(e) Wear at 5N, pH 5.5, high magnification

(f) Corrosion only, pH 5.5

(g) Wear at 5N, pH 9.7.

(h) Wear at 5N, pH 9.7.

(i) Wear at 5N, pH 9.7.

(j) Corrosion only, pH 9.7

(k) Wear at 5N, pH 15.5.

(l) Corrosion only, pH 9.7.

6. Schematic Pourbaix diagram for Ni-Cr/WC coating

7. Pourbaix diagram for Chromium.

8. Pourbaix diagram for Nickel

9. Schematic diagram showing the micro-abrasion-corrosion process.

10. Schematic diagram showing the micro-abrasion-corrosion mechanisms

11. Micro-abrasion-corrosion mechanism map for Ni-Cr/WC coating.

12. Wastage map for Ni-Cr/WC coating.

13. Additive-Synergy map for Ni-Cr/WC coating

14. Synergistic effects at pH 9.7

15. Synergistic effects at various pH values at -1.0 V

Table legends

I. Specifications of micro-abrasion apparatus

II. Experimental details

III. Mass loss data for micro-abrasion-corrosion interaction at -0.20 V

(a) pH 2 (b) pH 5.5 (c) pH 9.7 (d) pH 13.5

IV $\Delta Kc/\Delta Ka$ values at various pH values with fixed potential -0.2V

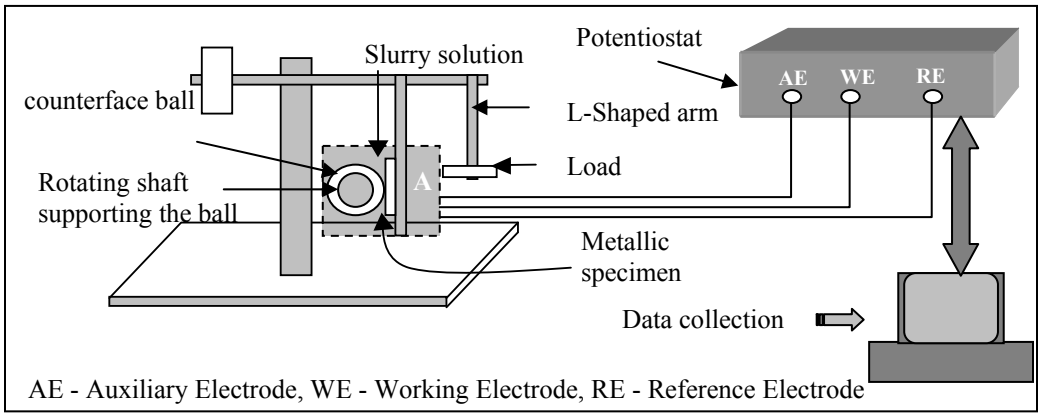

Figure 1

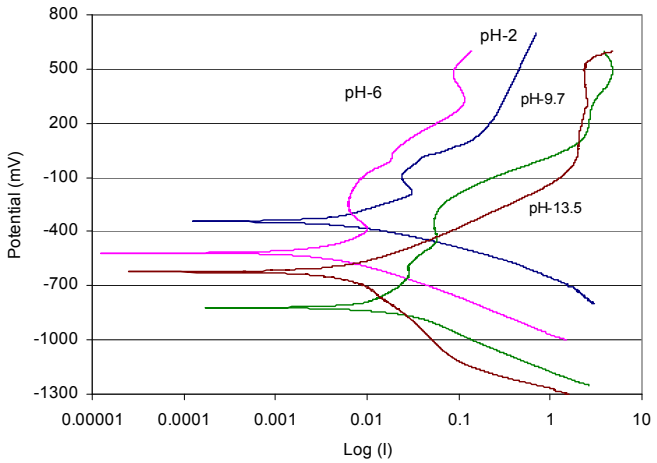

Figure 2(a)

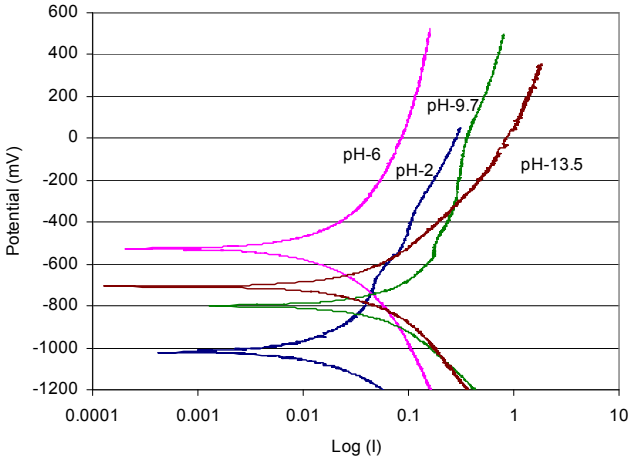

Figure 2(b)

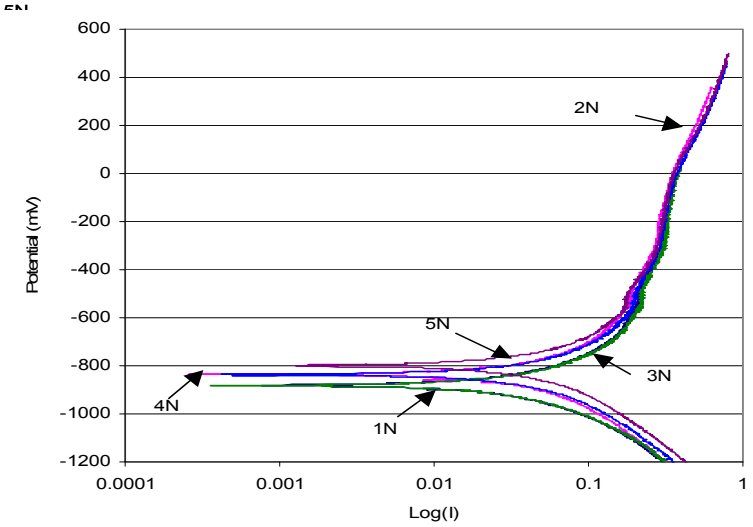

Figure 2(c)

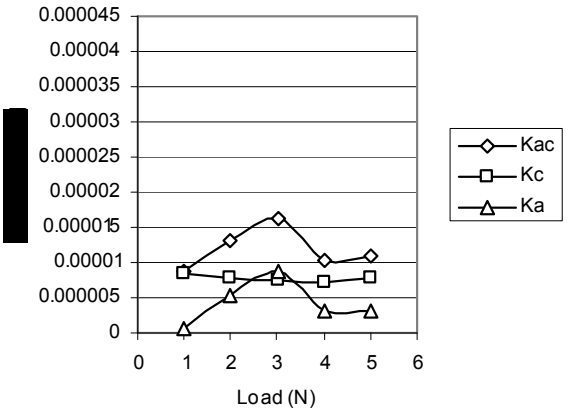

Figure 3(a)

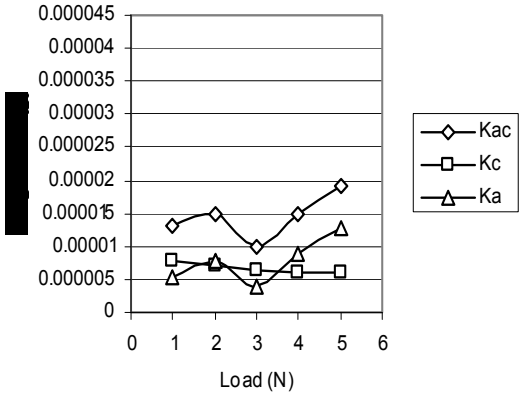

Figure 3(b)

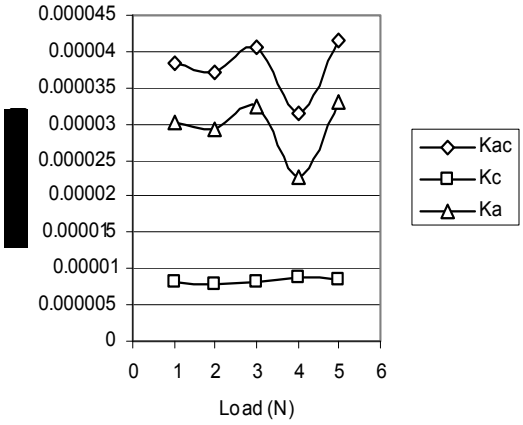

Figure 3(c)

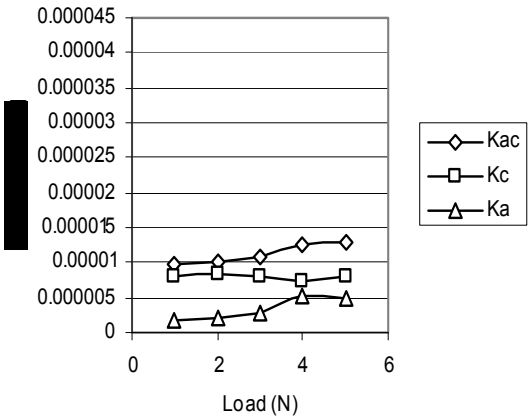

Figure 3(d)

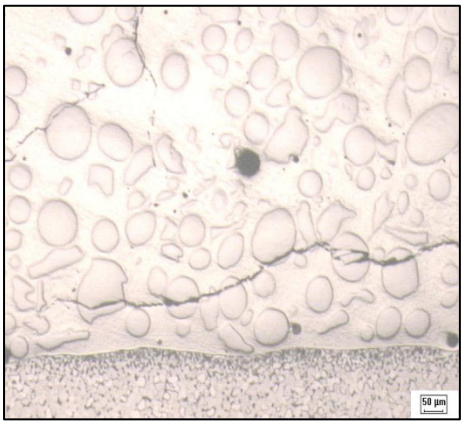

Figure 4(a)

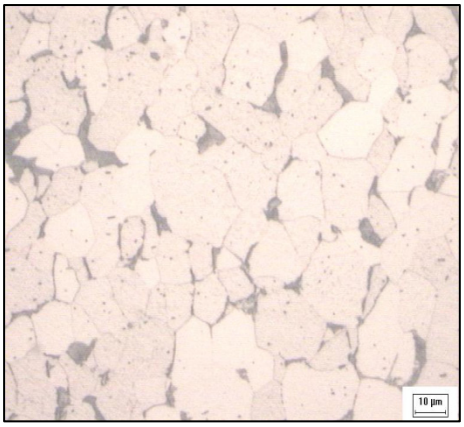

Figure 4(b)

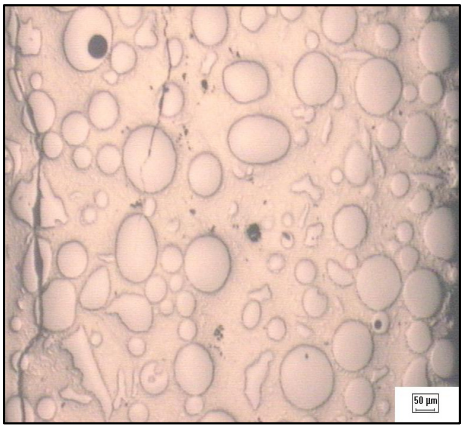

Figure 4(c)

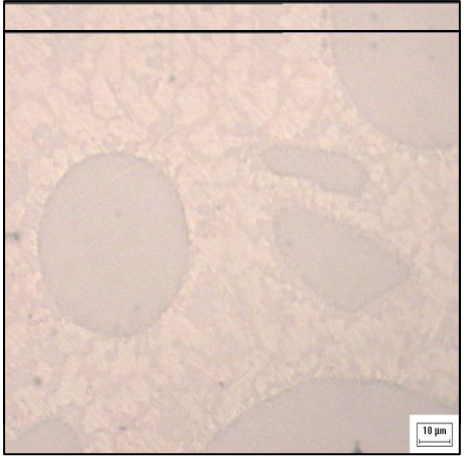

Figure 4(c)

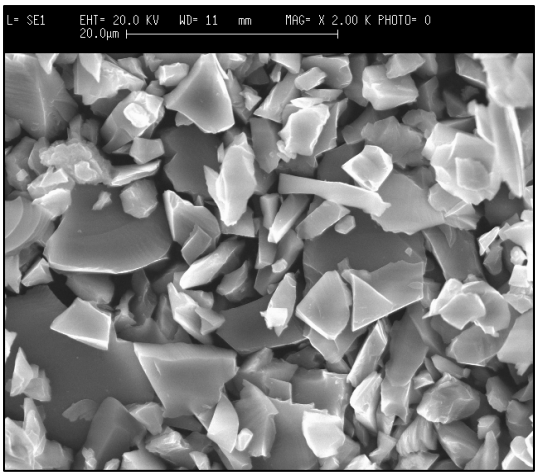

Figure 5 (a)

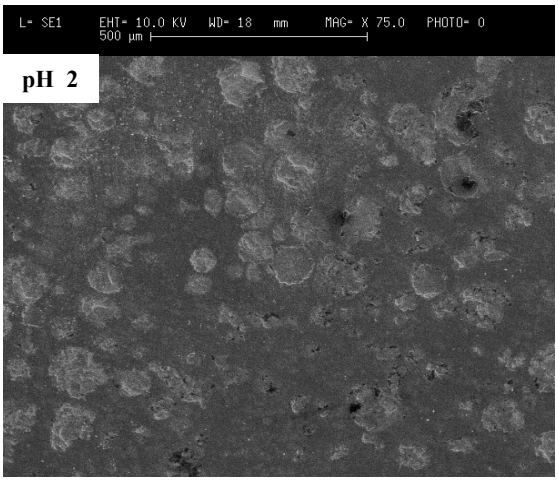

Figure 5 (b)

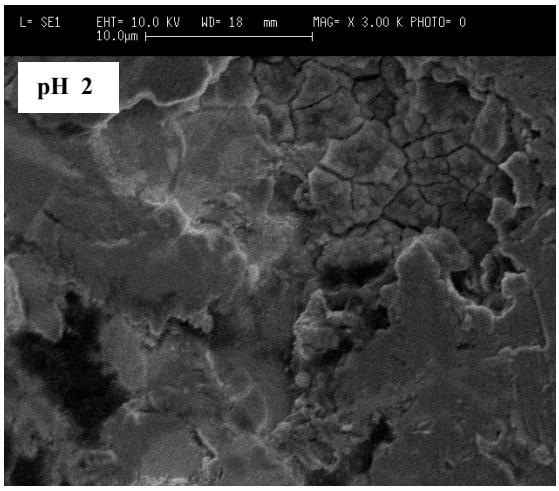

Figure 5 (c)

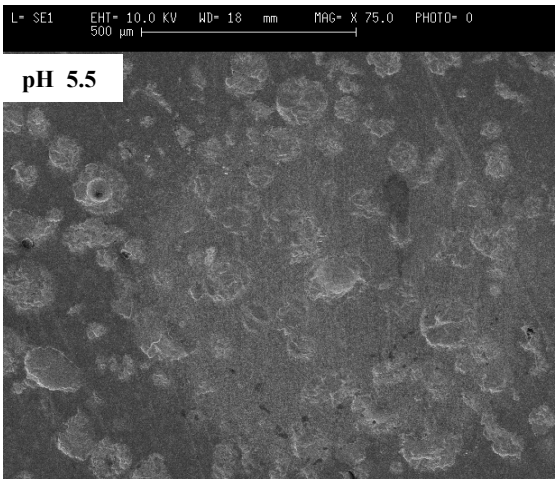

Figure 5 (d)

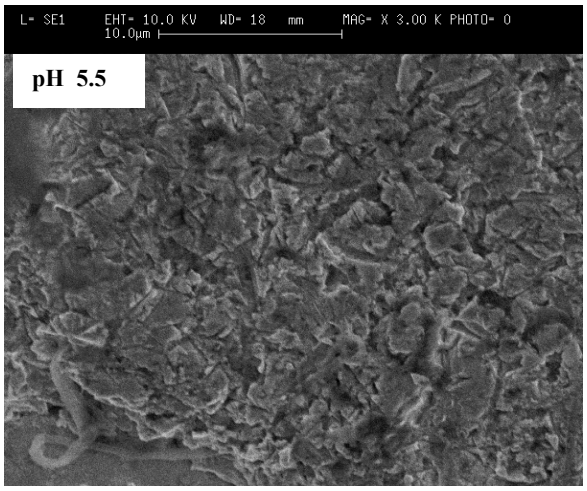

Figure 5 (e)

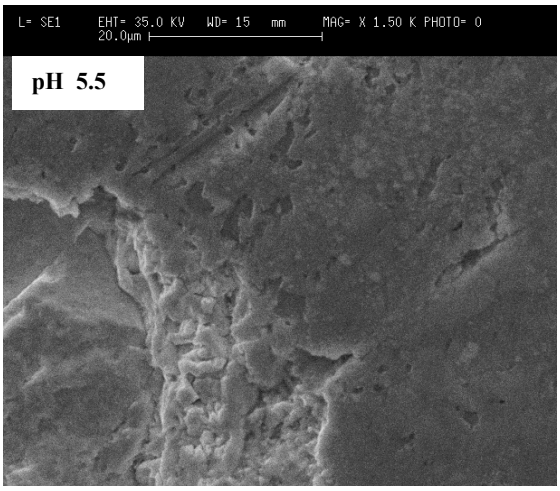

Figure 5 (f)

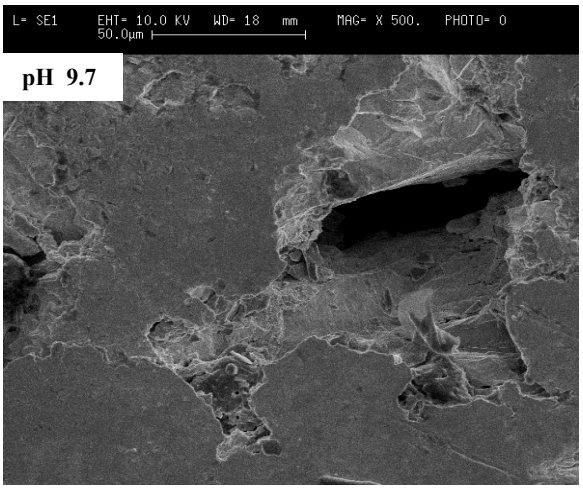

Figure 5 (g)

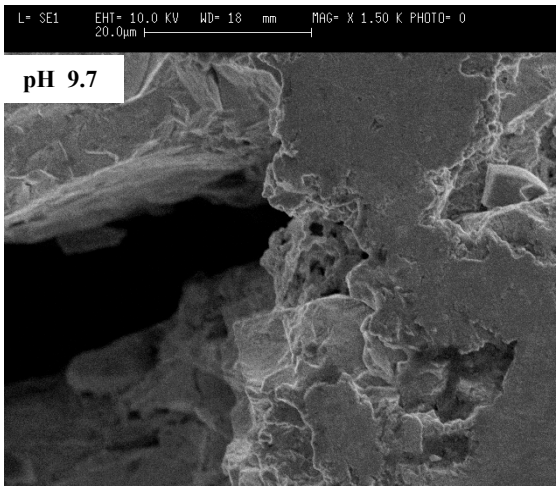

Figure 5 (h)

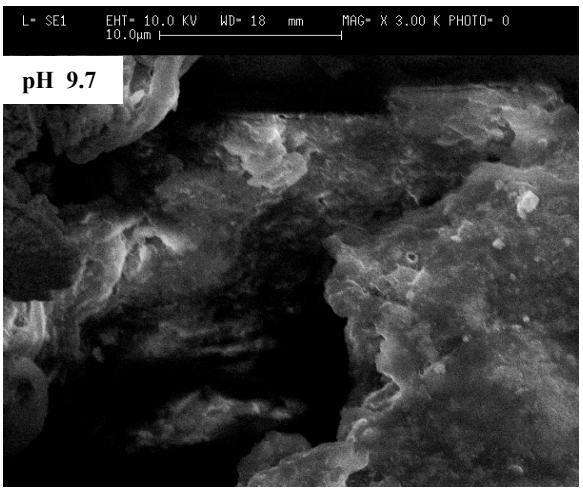

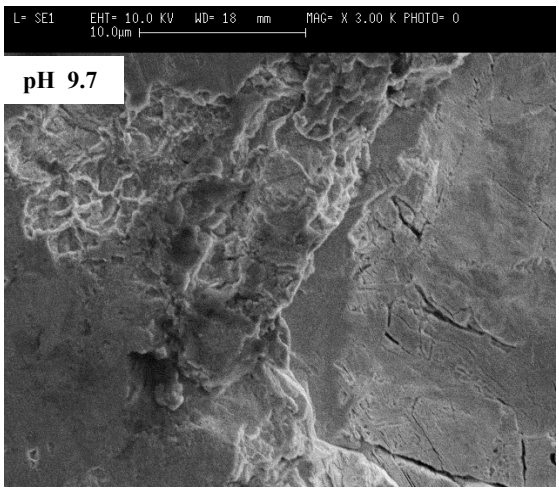

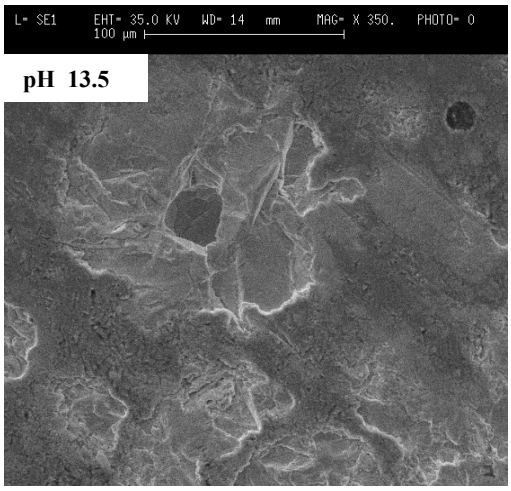

Figure 5 (k)

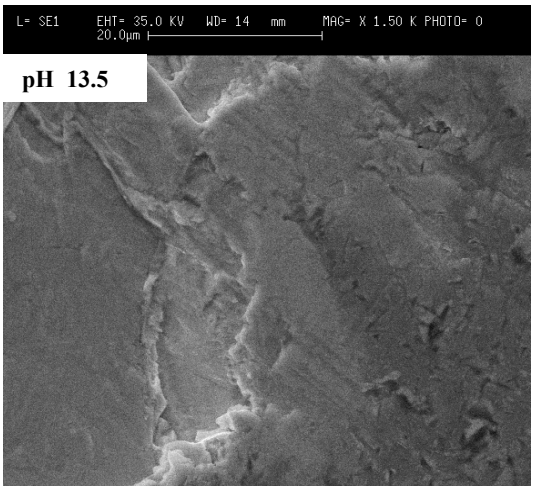

Figure 5 (l)

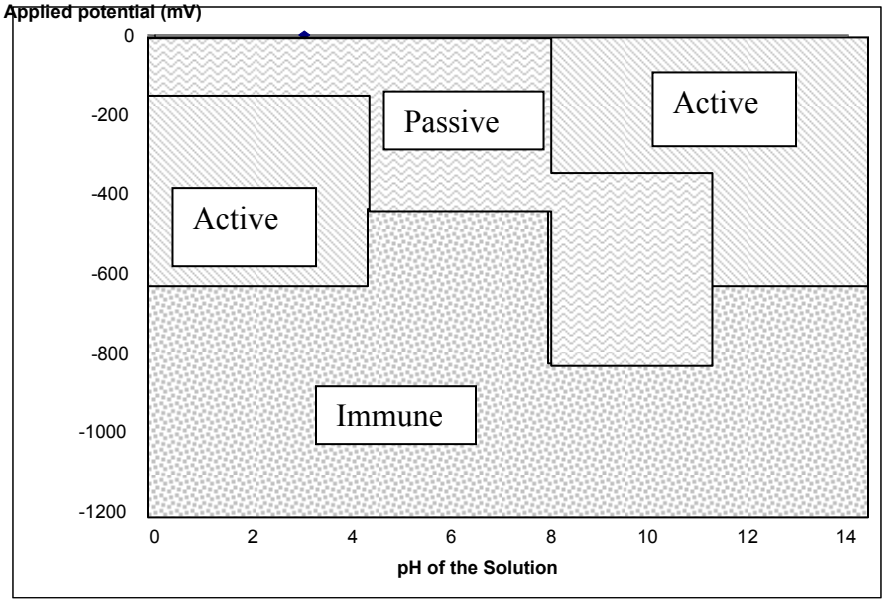

Figure 6

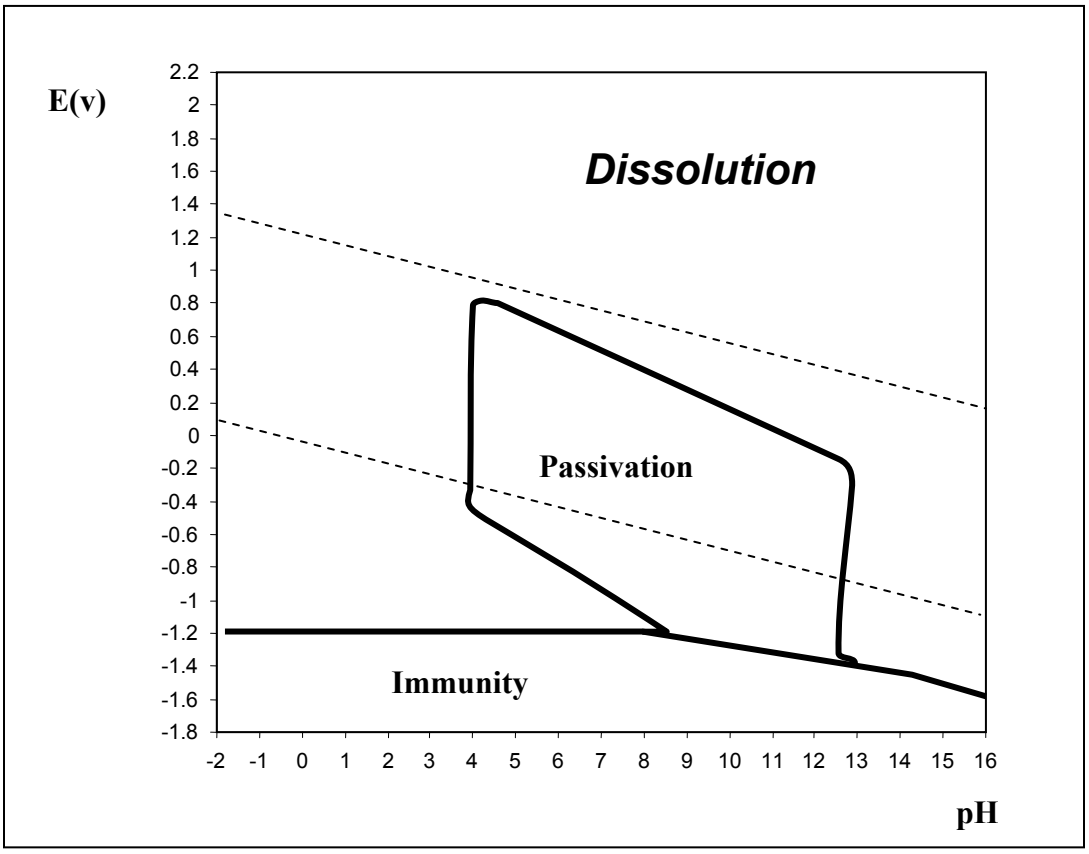
E(v)
Dissolution
Passivation
Immunity
pH

Fig.7

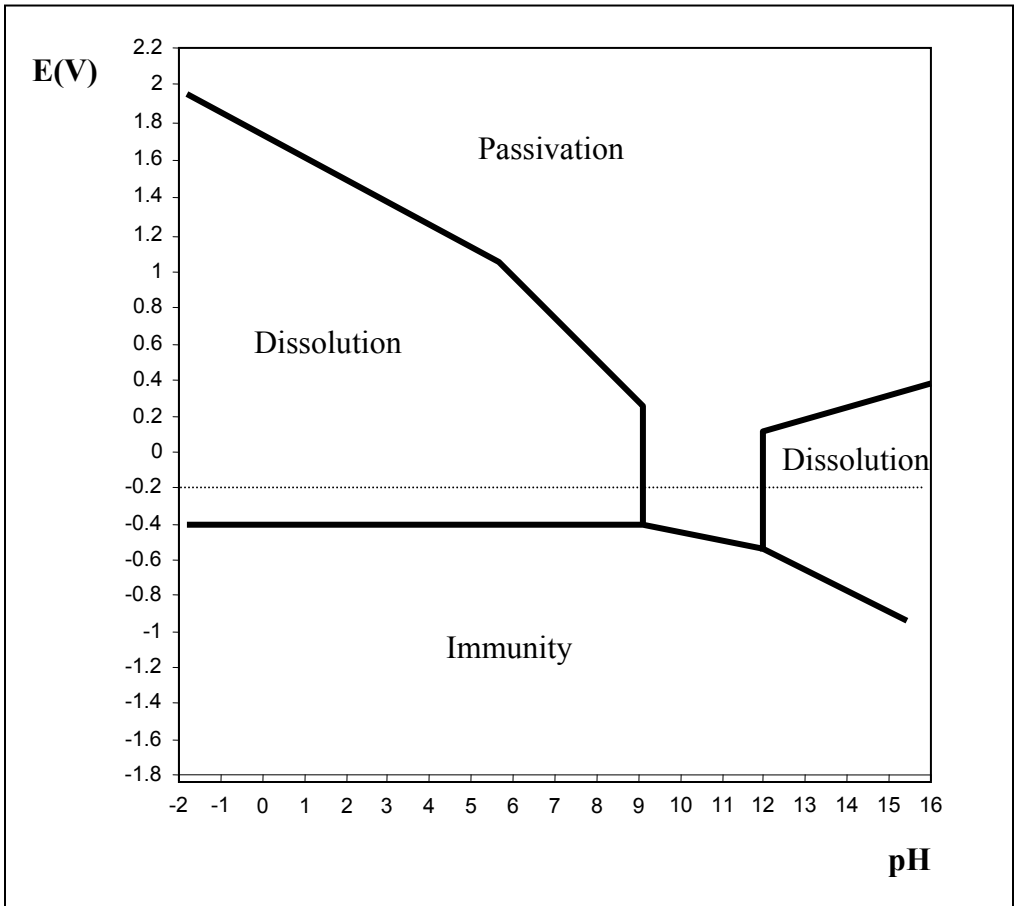
E(V)
Passivation
Dissolution
Dissolution
Immunity
pH

Fig. 8

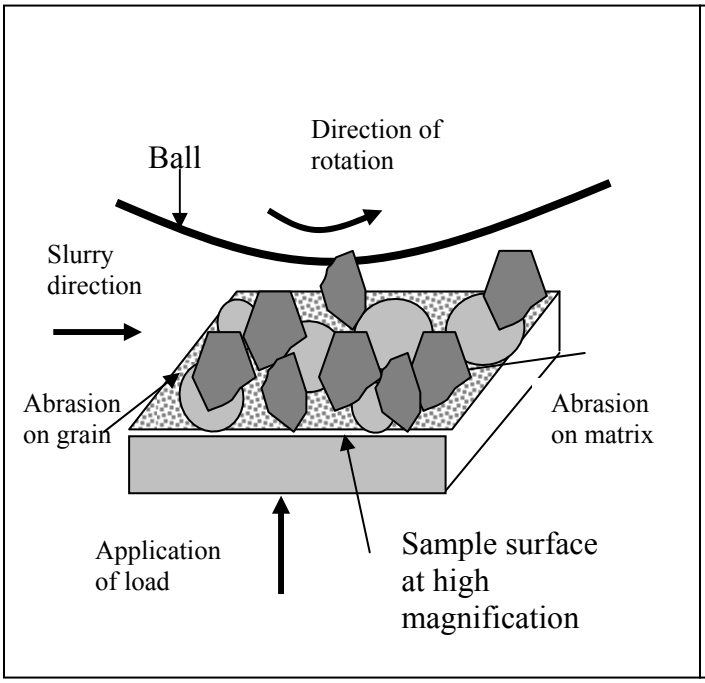

Figure 9

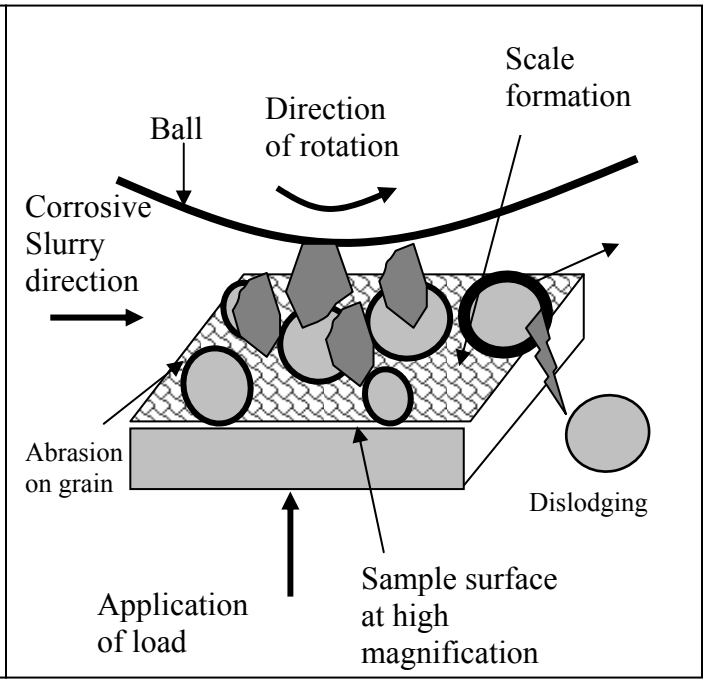

Figure 10

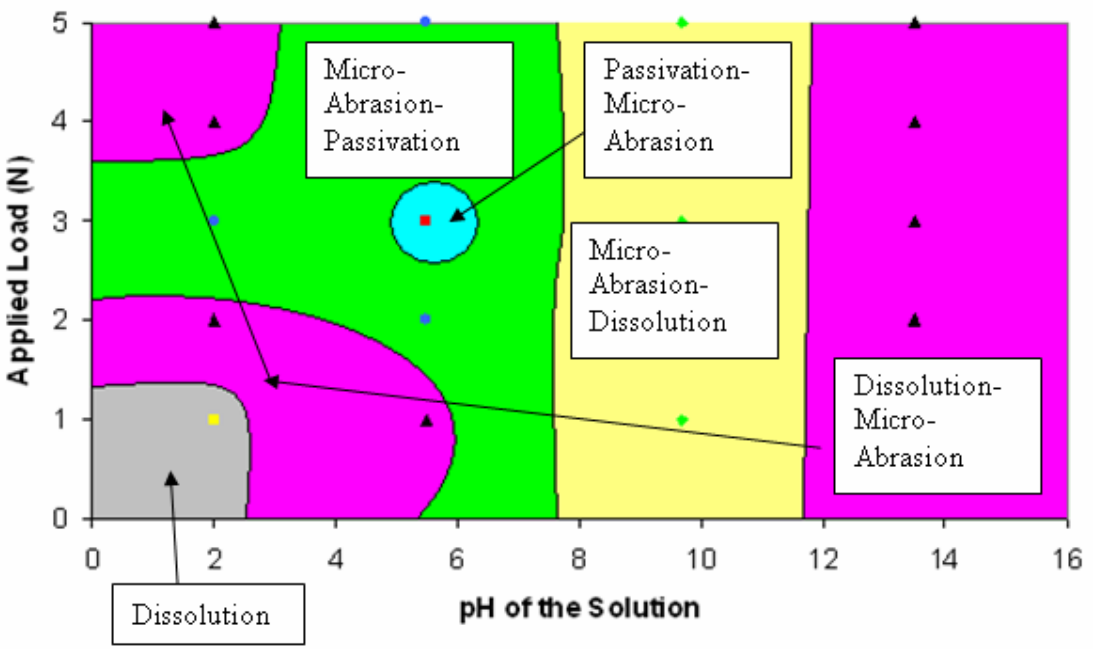

Figure 11

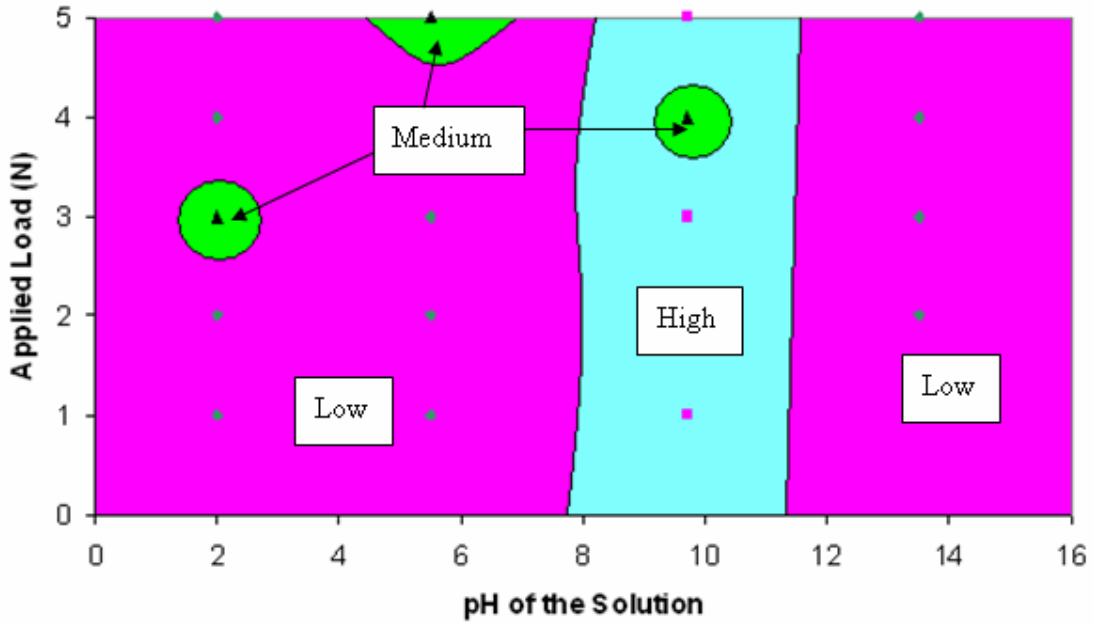

Figure 12

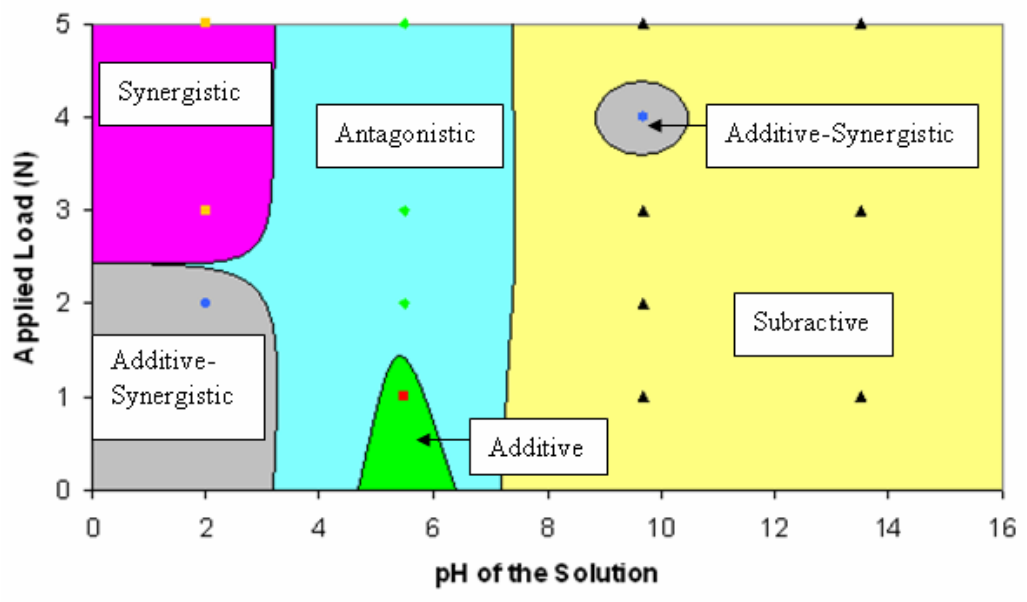

Figure 13

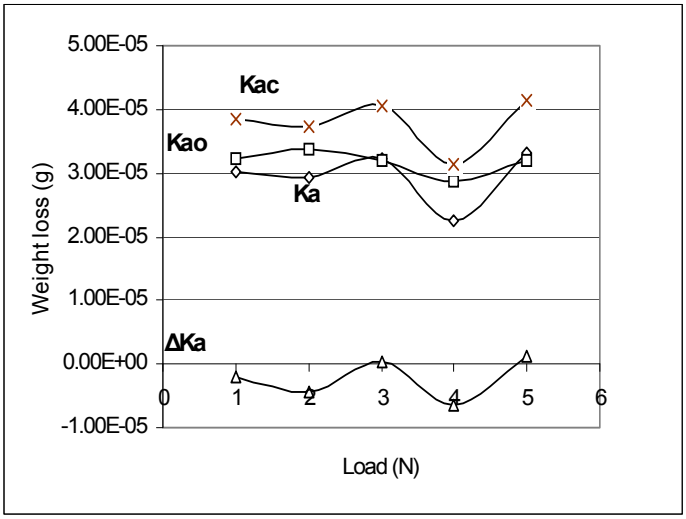

Figure 14

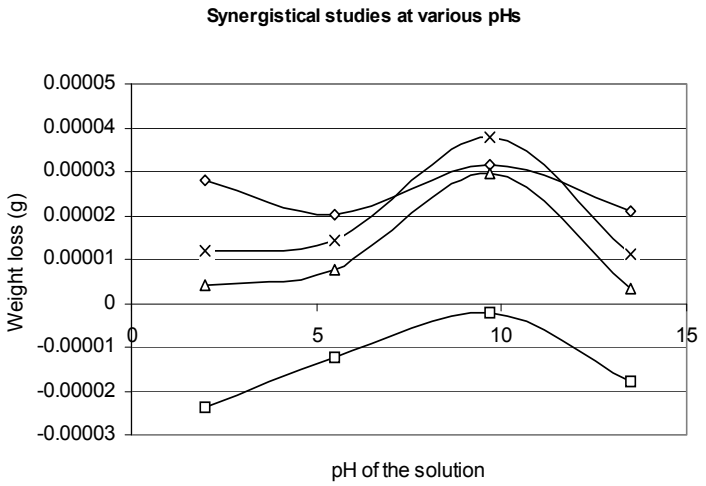
Synergistical studies at various pHs
0.00005
0.00004
0.00003
0.00002
0.00001
0
-0.00001
-0.00002
-0.00003
Weight loss (g)
0
5
10
15
pH of the solution

Figure 15

Table-1 Specification of the Micro-Abrasion apparatus	
Name & Model	Micro-abrasion tester, TE-66
Supplier	Phoenix tribology (Plint), UK.
Load range	0.05 to 5 N
Ball diameter	25 mm
Ball speed range	30 to 150 rpm
Pump feed rate	Up to 60ml h^{-1} (Based on 0.5mm bore)
Software Used	COMPEND 2000

Table-2 Experimental Details		
Sample Materials	Lasercarb WC coated mild steel	
Ball Materials	Ceramic (SiN)	
Speed	100RPM	
Load	1,2,3,4, and 5 N	
Sliding Distance	3000 Rev or (235.50 m)	
Slurry	Slurry composition: silicon carbide (4 μm diameter) with corrosive liquid (Concentration of 0.025g cm^{-3}). The composition of the solutions are as follows	
	pH	**Composition of liquid**
	2	Anhydrous sodium sulphate + sodium hydrogen sulphate monohydrate (0.5 M)
	5.5	Anhydrous sodium dihydrogen phosphate + anhydrous disodium hydrogen phosphate (0.5 M)
	9.7	Sodium bicarbonate + Sodium Carbonate (0.5 M)
	13.5	Potassium hydroxide (0.5 M)

Table 3a- Weight loss data for Micro-abrasion-corrosion interaction at fixed potential –0.2 V and pH 2						
Load (N)	Kac (g)	Kc (g)	Ka (g)	Kc/Ka	Kao (g) (Wear at –-1.0V)	ΔKa (g)
1	8.87 E-06	8.37 E-06	5.00 E-07	16.74	1.20 E-05	-1.15 E-05
2	1.32 E-05	7.84 E-06	5.36 E-06	1.46	1.30 E-05	-7.64 E-06
3	1.63 E-05	7.59 E-06	8.71 E-06	0.87	3.22 E-05	-2.34 E-05
4	1.02 E-05	7.04 E-06	3.16 E-06	2.23	3.32 E-05	-3.00 E-05
5	1.09 E-05	7.71 E-06	3.19 E-06	2.42	4.92 E-05	-4.60 E-05

Table 3b- Weight loss data for Micro-abrasion-corrosion interaction at fixed potential –0.2 V and pH 5.5						
Load (N)	Kac (g)	Kc (g)	Ka (g)	Kc/Ka	Kao (g) (Wear at –-1.0V)	ΔKa (g)
1	1.32 E-05	7.91 E-06	5.29 E-06	1.50	5.36 E-06	-7.00 E-08
2	1.49 E-05	6.99 E-06	7.91 E-06	0.88	2.73 E-05	-1.94 E-05
3	1.01 E-05	6.34 E-06	3.76 E-06	1.69	3.11 E-05	-2.73 E-05
4	1.48 E-05	6.08 E-06	8.72 E-06	0.70	1.14 E-05	-2.68 E-06
5	1.89 E-05	6.17 E-06	1.27 E-05	0.48	2.47 E-05	-1.20 E-05

Table 3c- Weight loss data for Micro-abrasion-corrosion interaction at fixed potential –0.2 V and pH 9.7						
Load (N)	Kac (g)	Kc (g)	Ka (g)	Kc/Ka	Kao (g) (Wear at –-1.0V)	ΔKa (g)
1	3.84 E-05	8.24 E-06	3.02 E-05	0.27	3.22 E-05	-2.04 E-06
2	3.72 E-05	7.95 E-06	2.93 E-05	0.27	3.36 E-05	-4.35 E-06
3	4.04 E-05	8.22 E-06	3.22 E-05	0.26	3.19 E-05	2.80 E-07
4	3.13 E-05	8.84 E-06	2.25 E-05	0.39	2.88 E-05	-6.34 E-06
5	4.16 E-05	8.44 E-06	3.32 E-05	0.25	3.19 E-05	1.26 E-06

Table 3d- Weight loss data for Micro-abrasion-corrosion interaction at fixed potential –0.2 V and pH 13.5						
Load (N)	Kac (g)	Kc (g)	Ka (g)	Kc/Ka	Kao (g) (Wear at –-1.0V)	ΔKa (g)
1	9.73 E-06	8.09 E-06	1.64 E-06	4.93	2.35 E-05	-2.19 E-05
2	1.03 E-05	8.32 E-06	1.98 E-06	4.20	2.29 E-05	-2.09 E-05
3	1.08 E-05	7.90 E-06	2.90 E-06	2.72	2.36 E-05	-2.07 E-05
4	1.25 E-05	7.17 E-06	5.33 E-06	1.35	1.04 E-05	-5.07 E-06
5	1.29 E-05	8.02 E-06	4.88 E-06	1.64	2.51 E-05	-2.02 E-05

Kc/Ka values at various pH values with fixed potential -0.2V

pH	Kac ($g \times 10^{-6}$)	Kc ($g \times 10^{-6}$)	Ka ($g \times 10^{-6}$)	Kc/Ka
(a) 1N Applied Load				
2	8.87	8.37	0.5	16.740
5.5	13.2	7.91	5.29	1.495
9.7	38.4	8.24	30.2	0.273
13.5	9.73	8.09	1.64	4.933
(b) 2N Applied Load				
2	13.2	7.84	5.36	1.463
5.5	14.9	6.99	7.91	0.884
9.7	37.2	7.95	29.3	0.271
13.5	10.3	8.32	1.98	4.202
(c) 3N Applied Load				
2	16.3	7.59	8.71	0.871
5.5	10.1	6.34	3.76	1.686
9.7	40.4	8.22	32.2	0.255
13.5	10.8	7.9	2.9	2.724
(d) 4N Applied Load				
2	10.2	7.04	3.16	2.228
5.5	14.8	6.08	8.72	0.697
9.7	31.3	8.84	22.5	0.393
13.5	12.5	7.17	5.33	1.345
(e) 5N Applied Load				
2	10.9	7.71	3.19	2.417
5.5	18.9	6.17	12.7	0.486
9.7	41.6	8.44	33.2	0.254
13.5	12.9	8.02	4.88	1.643

ΔKa/ΔKc values at various pH values with fixed potential -0.2V

pH	ΔKa ($g \times 10^{-6}$)	ΔKc ($g \times 10^{-6}$)	ΔKa/ΔKc	Effect
(a) 1N Applied Load				
2	-11.5	-19.49	0.590	Additive-Synergistic
5.5	-0.07	3.46	-0.020	Additive
9.7	-2.04	-44.27	0.046	Subractive
13.5	-21.9	-425.91	0.051	Subractive
(b) 2N Applied Load				
2	-7.64	-20.02	0.382	Additive-Synergistic
5.5	-19.4	2.54	-7.638	Antagonistic
9.7	-4.35	-44.56	0.098	Subractive
13.5	-20.9	-425.68	0.049	Subractive
(c) 3N Applied Load				
2	-23.4	-20.27	1.154	Synergistic
5.5	-27.3	1.89	-14.444	Antagonistic
9.7	0.28	-44.29	-0.006	Subractive
13.5	-20.7	-426.1	0.049	Subractive
(d) 4N Applied Load				
2	-30	-20.82	1.441	Synergistic
5.5	-2.68	1.63	-1.644	Antagonistic
9.7	-6.34	-43.67	0.145	Additive-Synergistic
13.5	-5.07	-426.83	0.012	Subractive
(e) 5N Applied Load				
2	-46	-20.15	2.283	Synergistic
5.5	-12	1.72	-6.977	Antagonistic
9.7	1.26	-44.07	-0.029	Subractive
13.5	-20.2	-425.98	0.047	Subractive